NUCLEAR INSTRUMENTS AND METHODS 164 (1979) 477-490, © NORTH-HOLLAND PUBLISHING CO

A SQUARE METER POSITION SENSITIVE PARALLEL PLATE DETECTOR FOR HEAVY IONS

D v HARRACH and H J SPECHT

Physikalisches Institut der Universitat Heidelberg, D-6900 Heidelberg, Germany

Received 30 April 1979

A parallel plate avalanche counter has been developed for the detection of time, x–y position and energy loss of heavy ions Construction and performance of prototypes with an active area of 26×26 cm^2 and of a final 1×1 m^2 version are described in detail The position determination uses a new principle based on a sense wire plane within the two parallel plate electrodes with a fast interpolating delay line read-out A time resolution of $\Delta t = 240$ ps (fwhm) and a position resolution of $\Delta x = \Delta y \leqslant 0.5$ mm (fwhm) are routinely obtained during actual experiments

1. Introduction

The availability of heavy ion beams up to U in recent years has led to an extended revival of gas filled detectors. Compared to semiconductor detectors, their main advantages are connected with large solid angles and the total insensitivity to radiation damage. As one example, the well known gridded ionization chamber has been extended to a position sensitive device with an active area of up to 12×40 cm^2 [1]), allowing – in inclusive measurements of binary reaction products – to simultaneously investigate Q-values, nucleon transfer and angular distributions with only one or a few counter settings.

Experiments of this type can alternatively be done as kinematic coincidences. Exclusive measurements of more complicated heavy ion reactions involving 3 or 4 heavy fragments in the outgoing channel necessitate even larger solid angles because of the large phase space available. Such reactions can be completely analyzed in terms of the total Q-value and all fragment masses by solely measuring the velocities (rather than energies) and angles of *all* reaction partners. Additional Z-information can be achieved in the usual way via the energy loss ΔE. The accuracy of the Q and m determination is ultimately limited by neutron evaporation. Experimentally, the mass resolution is essentially determined by the time-of-flight resolution. At a typical beam energy of 7 MeV/amu and a flight path of 1 m, an overall time resolution of 0.5 ns leads to a mass resolution of about 1.5%, whereas an angle resolution of about 2 mrad is sufficient for all purposes. A more detailed discussion of the complete experimental set-up and the accuracy limits in 3- and 4-body kinematic coincidence experiments is contained in refs. 2, 3. A quite general review of detection and identification problems in heavy ion reactions is given in ref. 4.

We have developed detectors with an active area of 1×1 m^2 specifically suited for this type of work. The basic trigger element, described in section 2.1, consists of a parallel plate avalanche counter. It combines a high count rate capability and a 100% detection efficiency with a time resolution of about 240 ps fwhm. Rather than to simply add an independent position sensitive detector like a Charpak counter or a drift chamber[5]), we have finally preferred to extract position information from the parallel plate detector itself. Our new principle[6]), described in detail in section 2.2, is based on a sense wire plane placed within the two main (foil-) electrodes and operated at half their potential difference. The signals sensed by these wires in proportion to their distance from the avalanche (without interference with the basic detector operation), are read out in an interpolating way by fast integrated-circuitry delay lines. Read-out system and delay lines are dealt with in sections 2.3 and 2.4, respectively. The sense wire principle, modified by charge division read-out, has more recently also been applied to a small (8×10 cm^2) transmission detector[7]). With a wire spacing of 2 mm, we have obtained a spatial resolution of $\leqslant 0.5$ mm fwhm, an integral linearity of ± 1 mm, and a differential linearity of 0.2 mm. The latter is limited by inhomogeneities of the delay lines. Two independent units of this type with crossed wire planes spaced 65 mm apart, provide the two orthogonal coordinates x and y, the space in between being used as a ΔE ionization chamber.

The whole system is usually operated at a pres-

sure of 5 torr heptane and a voltage of ~ 550 V, sealed off from vacuum by installation in a self-contained chamber with a thin (2.0 μm) mylar window. Construction and performance of 26×26 cm^2 prototypes and a 1×1 m^2 version are described in sections 3 and 4, respectively. Our exclusive measurements of 3- and 4-body heavy ion reactions nearly always involve more than one particle on a given detector unit. Section 5 is therefore devoted to a discussion of the double-event resolution and other problems associated with the data processing, done at present with a PDP 11/55 computer.

One of the 1×1 m^2 detectors has first been used in an investigation of sequential fission following deep inelastic collisions of Pb and U with a number of target nuclei from Ni to U. Examples of spectra demonstrating the actual on-line performance together with calibration procedures are contained in section 6, the final conclusions in section 7.

2. Basic detector characteristics

2.1. The trigger counter

Parallel plate avalanche counters (PPAC) first suggested by Christiansen[8]) and occasionally employed for protons[9-11]) have only recently been used in heavy ion physics[7,12-16]). Because of their constructional simplicity and excellent timing characteristics together with the high ionization density of heavy ions they appear to be by far the best choice for a large area trigger device. The basic operational principle consists of gas multiplication in a homogenous parallel electric field along the primary ionization track. With $n = \alpha d$, where α represents the first Townsend coefficient and d the gap width, the total gas multiplication of an electron starting at the cathode is given by

e^n,

the effective multiplication factor for the ion component of the pulse induced on the electrodes by[10])

$\approx e^n/n$,

and that of the electron component by[10])

$\approx e^n/n^2$.

The effective multiplication factor is smaller than the maximum value e^n, because primary ionization out of only 2 mean free ionization paths near the cathode contribute 75% to the resulting pulse, which in turn is generated essentially in the last 2 mean free paths near the anode. Thus, the main advantage of the counter – the fast, exponentially rising pulse with a well defined, nearly jitter-free delay relative to the ionizing event – is intimately connected to the main disadvantage – the poor ΔE resolution, restricted by straggling of the energy loss in a very thin layer.

With total differentiation of the slow ion part of the pulse, only the electron part is used for timing measurements. With the typical very large values of the reduced field strength of $E/p \sim 300-1000$ V/cm·torr at a pressure of ~ 5 torr, leading to large electron drift velocities and $n \approx 10$, rise times of <1 ns and time resolutions of 150–200 ps fwhm have been observed for small units (some cm^2) and a gap width of ~ 1 mm [12,14]). For larger areas (some 100 cm^2), the rise times degrade to 3–5 ns, but the time resolutions remain at about 200 ps. It appears at present, that the ultimate limits are not determined by rise times and signal-to-noise ratios, but by the fluctuations in the development of the avalanche[14]).

In a large detector, the propagation velocity of the signal is no longer negligable. Time delays of about 1 ns/20 cm have been found, enforcing a position determination in large counters for correction. The overall time resolution of a PPAC also sensitively depends on the homogeneity of the gap width. With a drift velocity of about 0.2–0.5 mm/ns (under the conditions given above), a gap width variation of 0.1 mm leads to a variation of the time delay between the ionizing event and the pulse of 200–500 ps. If again position is measured simultaneously, this can be corrected for by software.

2.2. Position measurement

One way to extract position information from the PPAC itself has been to subdivide the anode or cathode or both into geometrical regions like straight stripes[7]), concentric rings[13,16]) or other shapes[15]) specifically suited to the physical problem; these can then be read out independently[13,15]) or collectivity[7,16]). This scheme is especially useful for detectors with only one coordinate. Usually, the position electrode consists of a printed circuit board, but a pattern evaporated on a thin mylar foil in a transmission counter has also been used[7]).

For various reasons, we have developed a different approach. Placing an additional wire plane (or two) at an intermediate potential in between the two parallel plate electrodes (fig. 1), the position of

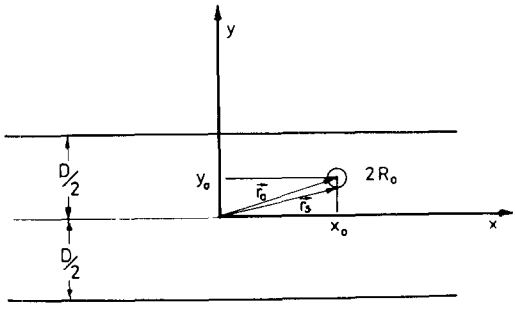

Fig. 1 Single wire of radius R_0 at position $r_0 = (x_0, y_0)$ between infinite parallel plates with a spacing D. r_s is a point on the wire surface

the ionization track can be sensed by the signals induced on these wires in proportion to their distance from the avalanche. Geometrically, this arrangement is similar to a multiwire proportional counter, but the operation is completely different with the wire plane acting solely as a "spectator" without participating in the avalanche multiplication process.

In the following, we will theoretically investigate

1) any possible disturbances of the avalanche by the wire plane leading to a degradation of the time resolution and the energy loss spectrum,
2) the differential linearity and spatial resolution associated with the interpolating character of such a system.

The discussion of the related electrostatic problem can be divided into two parts. The first deals with the actual distribution of the disturbed homogeneous field, the second with the detailed subdivision of the electric charges induced by the avalanche on the individual wires.

If a wire at a certain potential is placed into a homogeneous field, the field is disturbed (1) by the net charge of the wire, and (2) by the polarisation of the wire (and higher multipoles). If the potential of the wire is chosen to be the undisturbed value in its center, the net charge will be zero. The dipole field, on the other hand, never cancels. It depends on the undisturbed value of the field strength E_0 and the radius R_0 of the wire. The anisotropic distribution of the disturbing field ΔE around the wire has a maximum value of

$$\Delta E = E_0 (R_0/r)^2 .$$

Thus, at a distance of only 100 μm from a wire with a diameter of 20 μm, the relative disturbance has decreased to a level of 1%. For higher multipoles, the absolute values are still smaller and the radial fall-off is even faster. The same arguments basically hold in a multiwire arrangement.

The mathematical solution of the electric induction problem in a multi-conductor system should yield the dependence of the charges induced on all wires on an electron moving near the anode. The solution is found by applying the equivalence

$$\frac{dq^j}{q_0} = d\boldsymbol{r} \cdot \operatorname{grad} \frac{U^j}{U_0} .$$

The physical meaning of this equation is the following: If a point charge q_0 is displaced by $d\boldsymbol{r}$, the charge q^j induced on the jth conductor is changed by an amount dq^j. The potential U^j corresponds to that distribution for which the jth conductor has the potential U_0 and all others are grounded. The equivalence can be found by inspection of the electrostatic Green function.

The potential $U^j(r)$ can be deduced by the method of complex potentials. The real part for a single wire is given by

$$G(\boldsymbol{r}, \boldsymbol{r}_0) = G(x, y, x_0, y_0) = c \ln \times$$

$$\times \frac{\left\{\left[\sin \frac{\pi}{D} y - \sin \frac{\pi}{D} y_0 \cdot \cosh \frac{\pi}{D}(x - x_0)\right]^2 + \left[\cos \frac{\pi}{D} y_0 \cdot \sinh \frac{\pi}{D}(x - x_0)\right]^2\right\}^{\frac{1}{2}}}{\cos \frac{\pi}{D}(y + y_0) + \cosh \frac{\pi}{D}(x - x_0)} .$$

One has then to solve the system of linear equations

$$\sum q^k \, G(\boldsymbol{r}_s^{(l)}, \boldsymbol{r}_0^{(k)}) = U^l \qquad U^l = U_0 / jl ,$$

where U^l is the potential of the lth wire, on $\boldsymbol{r}_s^{(l)}$ a point on its surface and $\boldsymbol{r}_0^{(k)}$ is the position of the kth wire. The potential U^j is given by

$$U^j(r) = q^k \, G(\boldsymbol{r}, \boldsymbol{r}_0^{(k)}) .$$

This method can be refined by adding to the given monopole term a dipole, quadrupole or higher terms. The condition $U = \text{const.}$ can then be fulfilled for more than one point on the wire surface. These higher terms can, however, be neglected since the point of pulse formation $\boldsymbol{r}$ is far from the wire $|\boldsymbol{r} - \boldsymbol{r}_0| > R_0$.

It should be remembered that the rise of the parallel plate detector pulse occurs essentially very close to the anode. Thus, it is the normal derivation of the potential close to the anode which deter-

mines the induced pulse. If the wire spacing a is not too small compared to the electrode distance D and if R_0 is very small compared to D (see fig. 1): U^j near the anode is very similar to that of a single wire. The corrections are of the order

$$\ln\left(\tan\frac{\pi}{D}a\right)\Big/\ln\left(\tan\frac{\pi}{D}R_0\right)\approx 6\times10^{-3}.$$

If a wire is positioned at $y=0$, one can give $\partial U/\partial \boldsymbol{n}$ normal to the anode as

$$\left.\frac{\partial U}{\partial \boldsymbol{n}}\right|_{y=\frac{1}{2}D}\sim\cosh^{-1}\left(\pi\frac{x-x_0}{D}\right),$$

which is a bell-shaped curve as expected, whereas $\partial U/\partial \boldsymbol{n}|_{x=x_0}$ as a function of y is roughly constant. The results of this approximation are given in fig. 2.

Assuming the same spatial dependence for all avalanches and a small extention of the avalanche in the x, y plane, the distribution of the induced charge as a function of the distance from the jth wire is then similarly given by

$$q^j\sim\cosh^{-1}\left(\pi\frac{x-x^j}{D}\right).$$

This situation is illustrated in fig. 3.

We can now also calculate the center of gravity $\bar{x}$ of this distribution and compare it to the actual value x. Symmetry imposes the condition $\bar{x}=x$ on the wire and just in the middle between two wires. Fig. 4 shows the results from a calculation for $a=2$ mm and $D=3$ mm which apply to the detectors actually built. Further results are given for $a=1$ mm and $a=1.5$ mm. The differential linearity yields a maximum deviation $(\bar{x}-x)_{\max}$ of 56 μm for $a=2$ mm.

Another way of looking at the same problem is to plot the quantity $\mathrm{d}\bar{x}/\mathrm{d}x$, which describes the transformation of an intensity distribution (fig. 5).

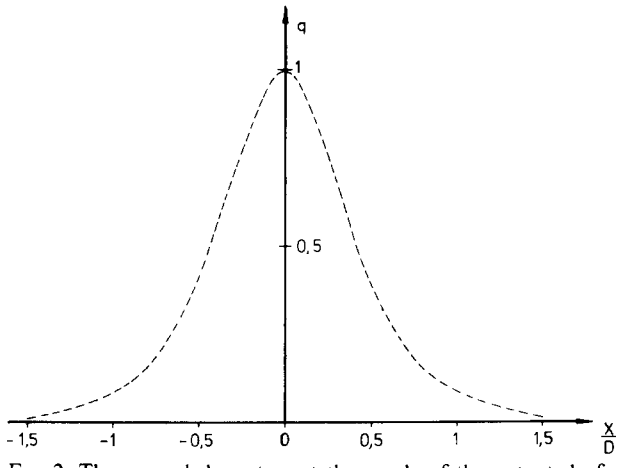

Fig. 2 The normal derivative at the anode of the potential of a single wire located at $x_0=y_0=0$ between parallel plates of distance D. The curve is normalized to 1 at $x=0$

If, for instance, all x are equally distributed as a "white" position spectrum $W(x)$, the transformed spectrum $W(\bar{x})$ – proportional to $\mathrm{d}\bar{x}/\mathrm{d}x$ – will have a modulation of $=\pm16\%$ for the present 2/3 geometry. Such variations can, of course, be reduced by reducing a/D.

Since the total induced charge is shared between the cathode and the wire system, position-dependent fluctuations exist in the amount of charge on the wire system alone. In the example presented they are of the order of $\pm3.5\%$. These variations are illustrated in the upper part of fig. 4.

2.3. Read-out

Two principally different methods exist for determining the average position $\bar{x}$. In the first, all q^j are measured separately and $\bar{x}$ is deduced by computational methods. In the second, a collective read-out scheme is used which performs most of the averaging inherently. The individual scheme is fast and allows very high counting rates, but necessitates

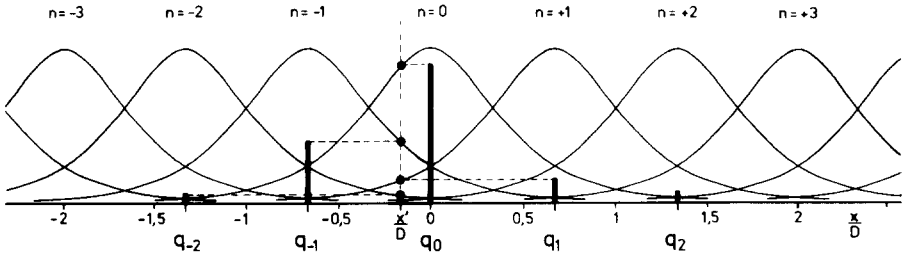

Fig 3 Distribution of influenced charges on neighbouring wires by a charge moving at x'/D near the anode The geometry $D=3$ mm, $a=2$ mm corresponds to that actually used The black bars denote the position of the wires and the magnitude of the influenced charge

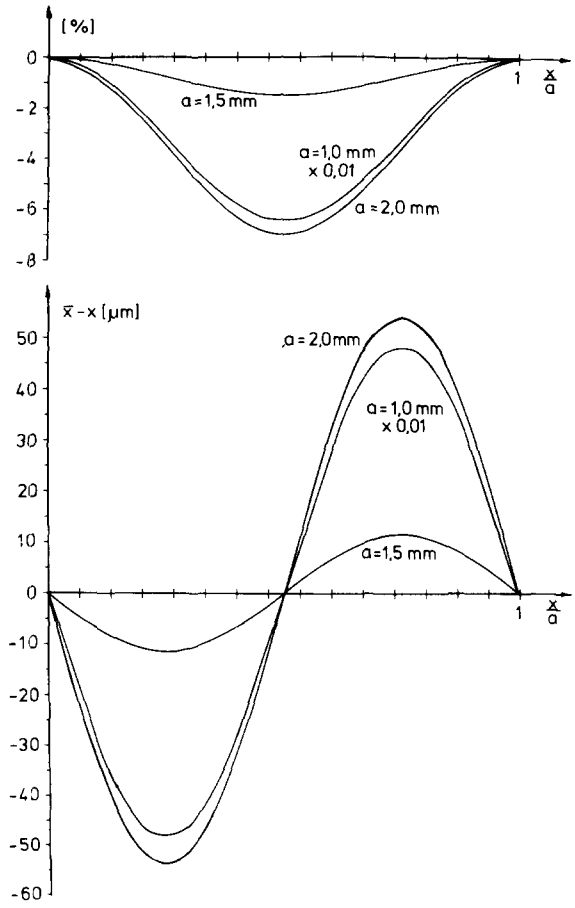

Fig 4 Upper part: dependence of the summed influenced charge on the position x/a for different geometries ($a/D = 2/3$, 1/2, 1/3). Lower part deviation of the center of gravity of the influenced charges from the actual position in microns for the same geometries

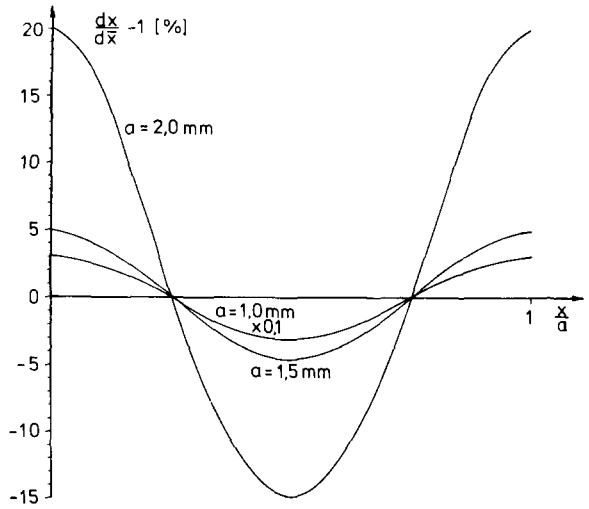

Fig 5 Intensity modulations in percent as a function of position for different geometries ($a/D = 2/3$, 1/2, 1/3). These modulations can be large even if $\bar{x}-x$ is small

amplifiers and ADCs separately for each wire. In the collective scheme, less electronics is needed at the expense of smaller counting rates.

Collective read-out can be achieved either by current division, coupling the wires to a resistor chain, or by employing delay lines, coupling the wires to an L–C chain. In the current division method, the charge collected at one end of the chain is compared to the sum of the charges from both ends, generating the coordinate $\bar{x}$ by division. In the delay line method, the measurement of only the time difference between the signals at the two ends yields the coordinate directly.

We have preferred the delay line read-out for the following reasons:

1) Speed: for a delay of 1 ns/mm and a wire group of 25 cm, the maximum delay time of 250 ns allows statistical counting rates of up to 500 kHz.
2) Economics: collective groups of >100 wires can be read out with a minimum of electronics and no degradation in resolution.
3) Redundancy: in an addition to the time difference $t_2 - t_1$, also the absolute times between the fast anode pulse of the parallel plate detector and the two delay line signals can be used for coordinate determination. The sum of these additional parameters must correspond to the total delay. If it does not, a double event has taken place which can either be rejected or treated differently.

To demonstrate the equivalence of delay line coupling and the desired interpolating determination of $\bar{x}$, we consider a Taylor expansion of the time dependence of the induced signal

$$f(t) = f(0) + \left.\frac{\mathrm{d}f}{\mathrm{d}t}\right|_{t=0} \cdot t + \ldots .$$

The time dependence of the delay line signal corresponds to

$$F(t) = \sum q^j f(t - j\tau),$$

where τ represents the characteristic delay between two consecutive wires. By insertion and resummation

$$F(t) = (\sum q^j)\left[f(0) + \left.\frac{\mathrm{d}f}{\mathrm{d}t}\right|_{t=0} \cdot \left(t - \frac{\tau \sum jaq^j}{a \sum q^j}\right) + \ldots\right]$$

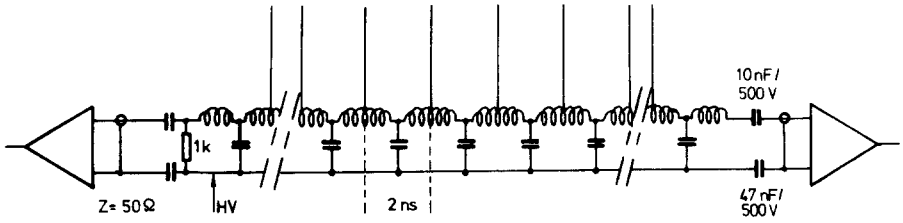

Fig. 6. Delay line with direct coupled wires at L/2 The capacitors (10,47 nF) are used for coupling of signals from the delay line which has a potential of +300 V The delay-line, the cables and the amplifier have an impedance of 50 Ω. The delay per tap is 2 ns.

is obtained, which can be interpreted as being proportional to the function

$$f\left(t-\frac{\tau}{a}\bar{x}\right),$$

thus yielding the desired quantity $\bar{x}$ as a time delay.

Clearly, this averaging is only meaningful, if the characteristic delay τ multiplied by the half-width of the q' distribution is comparable to or smaller than the rise time of the delay line signals. Such a condition can also be enforced by additional filtering.

2.4. Delay lines

The main characteristics of a delay line are determined by its impedance $Z=\sqrt{(L/C)}$ and the delay per tap $\tau=\sqrt{LC}$. Comparing the two methods of coupling wires to a delay line, i.e. capacitive coupling and direct coupling, we have preferred direct coupling for simplicity. In this case, a combination of ceramic capacitors and high quality inductances gives a homogenous delay line with any number of taps. The choice of 33 pF capacitors and 0.15 μH inductances yields $Z=67.4\,\Omega$ and $\tau=2.22$ ns. Alternatively, we have also used tapped delay line packages (10 taps per module) with $Z=50\,\Omega$ and $\tau=2$ ns from different manufacturers. Usually, homogenity presents a problem especially at the junction of two modules. L/2–C–L/2 combinations instead of ordinary L–C combinations seem to be superior in this sense. At present, the read-out is done with one delay line (11–13 modules) for 110–130 wires (see fig. 6).

The impedance has been chosen to be close to 50 Ω to simplify the direct connection to preamplifiers with ordinary 50 Ω cables over distances of several meters. Use of low impedances also renders the characteristics of the delay line less sensitive to stray capacitance If long wires with a capacitance C_s are connected, one has

$$Z=Z_0(1+C_s/C_0)^{-\frac{1}{2}} \quad \text{and} \quad \tau=\tau(1+C_s/C_0)^{\frac{1}{2}}.$$

Changes are smallest for large C_0 which implies low impedance. In addition delay lines of low impedance are physically small because of the small capacitors, whereas low loss inductances have large volumes.

The characteristic delay τ was chosen to be 2 ns for the following reasons:

1) The delay per mm should be comparable to or larger than the differences of the propagation times of the anode signals in the parallel plate system. Under these circumstances, the time difference between anode signals and delay line signals can be used as a good approximation to the coordinate.
2) The total delay should be as short as possible in order to have a fast recovery time for high counting rates.

3. Construction and performance of prototypes

Following the principles discussed above, prototypes with an active area of 26×26 cm^2 have been built. One module (fig. 7) consists of two equivalent counters, each containing one wire plane. They are mounted back to back with a 90° orientation of the wire direction, the inner planes being the grounded cathode planes. The space between the cathodes is expanded to 5 cm; it serves – together with a collection grid – as a transmission ionization chamber. Extreme care has to be taken to minimize cross talk problems between the independent detector sections.

The x and y counters are made out of two aluminized mylar foils with a thickness of 1.5 μm and a resistance of 1 Ω/□. The foils are stretched and glued to epoxy frames which also contain the contacts. The distance of the electrodes is defined by two additional epoxy frames with a thickness of 1.5 mm each. One of these frames is a printed circuit board, also carrying the wire system and the

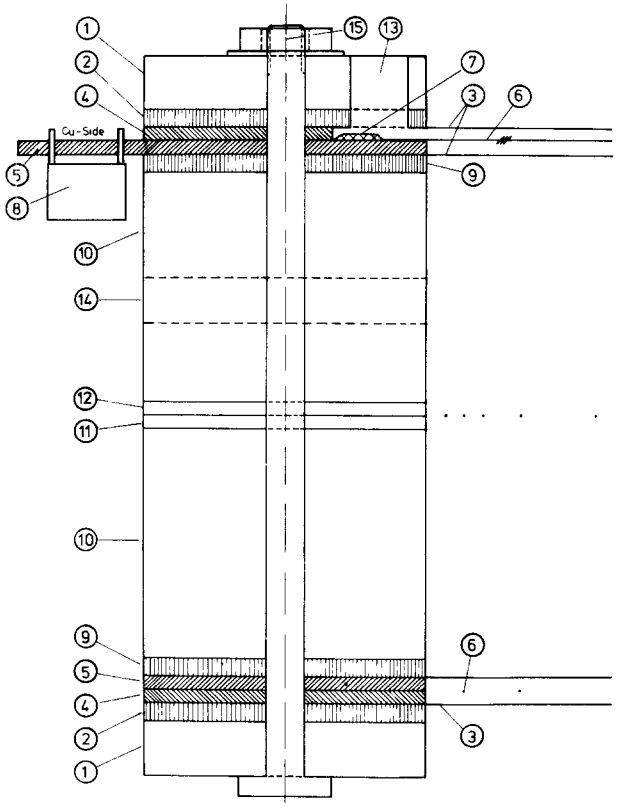

Fig 7 Schematic cut through a counter module The numbers correspond to (1) outer frames for packaging, glass-fiber epoxy 6 mm thick, (2) anode frames glass-fiber epoxy 2 mm thick, (3) aluminized mylar foil, 2 μm, 1 $\Omega/\square$, (4) spacer 1 5 mm glass-fiber epoxy, (5) wire frame with photoetched contact pattern; 1 5 mm, (6) wires 20 μm gold-plated tungsten, (7) solder for electrical contact and mechanical fastening, (8) delayline DIP (Rhombus TZB 12-5), (9) cathode frame, (10) Lucite spacer 25 mm, (11) spacer 1 5 mm glass-fiber epoxy, (12) wire frame, collection grid of ionization chamber 20 μm gold-plated tungsten wires spaced 2 mm, (13, 14) gas inlet (outlet), (15) steel bolt for clamping

delay line. 20 μm gold plated tungsten wires are used, soldered to the printed circuit board at a spacing of 2 mm and a tension of 30 P. Thus, the geometry of $a = 2$ mm, $D = 3$ mm discussed above is realized.

The three detector sections x–ΔE–y are clamped together with two additional epoxy frames, resulting in a stiff package of three nearly gas tight volumes, each with its own gas in- and outlet. The combined module is contained in a chamber with a mylar entrance window on the front side. Mylar foils of 2 μm supported by a grid of 100 μm Wo wires with a mesh width of 1×1 cm^2 hold a pressure difference of about 50 torr.

As counting gases, butane to heptane with pressures ranging from 3 to 20 torr have been investigated, hexane at 5 torr being used at present. Under these conditions a voltage of about +600 V has to be applied to the anode, +300 V (by voltage division) to the wire plane. Consequently, the signals have to be decoupled by capacitors; this is done within the gas volume. Thus, 7 signals and 2 supply voltages finally have to be connected:

counter 1 : right–left end of delay line, anode 1,
ΔE : collection grid,
counter 2 : upper–lower end of delay line, anode 2.

From these signals, several parameters can be deduced in a redundant way:

1) Each delay line together with the anode signal gives three different coordinates, i.e.

$$T_R = t_{right} - t_{anode},$$

$$T_L = t_{left} - t_{anode},$$

$$T_{RL} = t_{right} - t_{left}.$$

As mentioned above, this allows for recognition of double events.

2) Two trigger signals are available. It is therefore possible to determine the time resolution with single events, to reject signals from other than heavy particles (electrons, gammas, sparks), and to exploit a TOF signal with 5 cm flight path.

The collection grid of the ionization chamber carries a potential of −200 V, thereby saturating the drift velocity at low pressures with resulting pulse rise times of about 0.5 μs. A charge sensitive preamplifier is used together with a spectroscopy amplifier, leading to best results with a shaping time of 0.5 μs. One should keep in mind that the ion signal is not decoupled by a Frisch-grid, and that the pulse height corresponds to only one half of the energy loss in the detector volume.

Measurements have been performed with α- and fission sources and different heavy ion beams, ranging from ^{16}O to ^{208}Pb at count rates up to 500 KHz.

With α-particles and 15 torr hexane as counter gas, the chamber can be operated at 650 V the pulse height of the electron component is then about 1–5 mV with a rise time of 3 ns (measured at 50 Ω). The signals are further amplified by roughly a factor of 300 and then fed into a constant fraction trigger (CFT). The time resolution is observed locally to be 300 ps for α-particles and 220–240 ps for

heavier particles. With highly ionizing particles and high count rates, the supply voltage has to be lowered. As one example, for 400 kHz Xe-ions the chamber was operated at only 480 V (roughly speaking each 20 V correspond to a factor 2 in pulse height), but still retained a time resolution of 220 ps.

If the anode signals are picked off at the same corner of the module no geometrical correction has to be applied to the time difference of the two anode signals. The time resolution for monoenergetic particles then depends only on the homogeneity of the gap width. Electrode foils must be stretched properly since electrostatic forces tend to reduce the gap width in the center of the counter. Gas flow should be held constant since varying flow results in pressure differences across the electrodes. Without correction for propagation delays, overall time resolutions of 350–500 ps can be achieved.

The signals from the delay line are about half of the anode signals, but of opposite polarity. Rise times vary between 5 and 15 ns, depending on particle position. Additional R–C filtering can be used to narrow the rise time distribution. After inversion and amplification, the signals are fed into CFTs operating with a fraction 0.5 and compensating for rise time and pulse height variations. Integral linearity is found to be better than 1 mm over a distance of 15 cm. The spatial resolution is close to 0.5 mm fwhm, using well collimated α-particles. The differential linearity mirrors the $d\bar{x}/dx$ intensity distribution from the averaging procedure. The expected $\pm 16\%$ modulation is, in fact, confirmed in the position spectra.

As a more stringent on-line test, kinematic coinci-

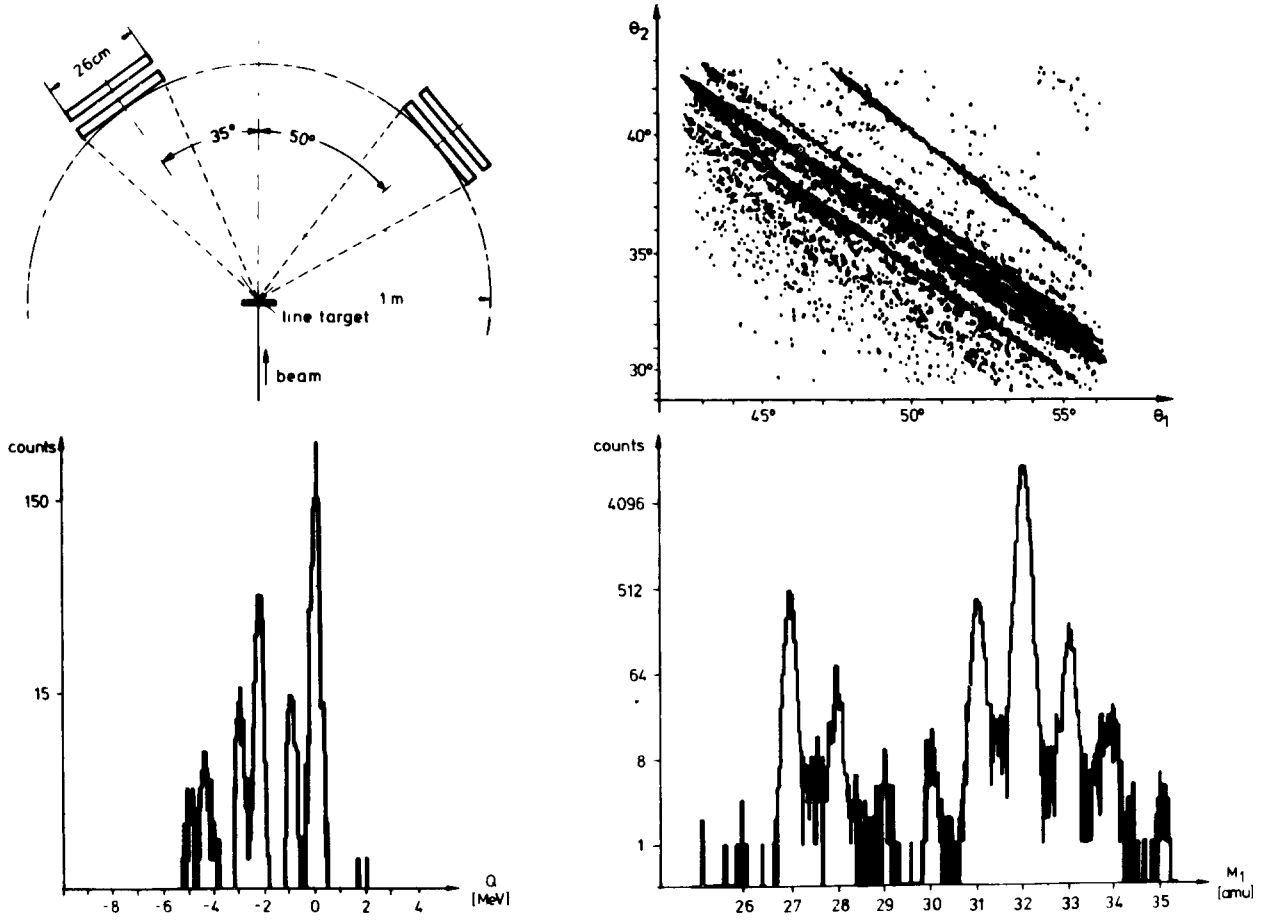

Fig 8 Kinematic coincidences in the system 85 MeV $^{32}S \rightarrow {}^{27}Al$ with two prototype counters (a) Schematic set-up, (b) θ_1 θ_2 correlation diagram, (c) mass spectrum, the resolution is 0 3 amu, (d) excitation spectrum of inelastic scattering The half-width is 150 kV The non-Gaussian line shape is due to multiple scattering in the target

dences have been measured with two such detectors for the binary system $^{27}Al(^{32}S,x)y$ at $E_{lab} = 85$ MeV [17]). The experimental set-up and examples for a mass and Q-spectrum are shown in fig. 8. Using a 10 μg/cm^2 Al target and a flight path of 1 m for each detector, a Q-value resolution of 150 keV fwhm and a mass resolution of 0.35 amu fwhm have been achieved. This again corresponds to a time resolution of 350 ps and a spatial resolution of 0.5 mm. In these measurements, the whole active area of both detectors was used without any software position–time correction.

4. Construction and performance of a 1×1 m^2 detector

For a number of reasons, our square meter detector is divided into subsections. With increasing detector area

1) pulse heights and rise times degrade,
2) the collective read-out suffers from more chance coincidences,
3) the recognition and analysis of real double events becomes much more difficult,
4) mechanical stability against acoustic vibrations and electrostatic forces enforce additional support in any case.

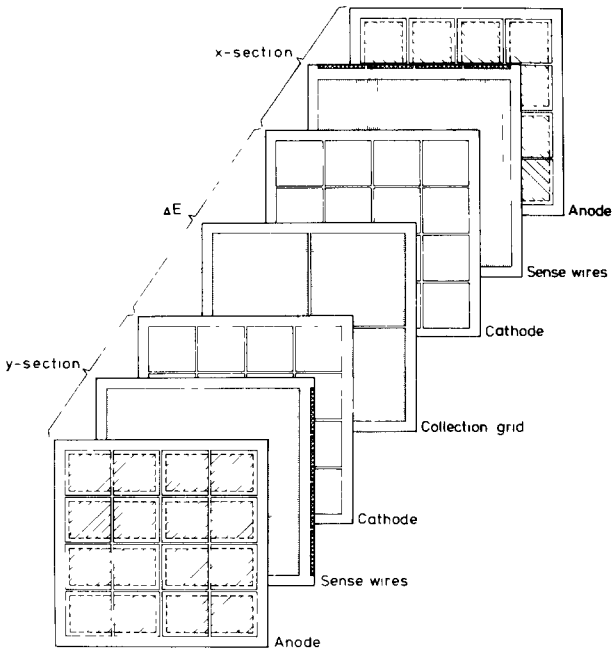

Fig 9 Schematic view of the square meter counter with the x-section facing the target, followed by the ΔE- and the y-section The subdivision of the anodes is indicated by the dashed lines The cross hatched bars on the sense wire planes indicate the 2×4 delay line sections each for the collective read-out of 110 wires The grounded cathodes are not subdivided; thus crosstalk to the ΔE-sections is reduced

Since electrode foils of a transmission counter can only be contacted on the outer frames, a division of the detector into $2 \times 4 = 8$ submodules has been chosen. The whole arrangement is schematically illustrated in fig. 9. Each rectangular module has a common side with the outer frame. The longer side of the rectangles corresponds to the direction of the wires (now with a length of 1 m), the smaller side to the length of one delay line. Four delay lines therefore have to be used. The area 22×44 cm^2 of one sub-module is comparable to that of the prototypes. Gap width and wire separation are also kept at 3 and 2 mm, respectively. Two such units are again mounted back to back at a 90° orientation of the wire planes. The collection grid of the ΔE ionization chamber in between is divided in 8 submodules as well.

Since greater mechanical stability is necessary, the electrode foils are glued to glass fiber epoxy (G II) frames machined out of sheet material with a thickness of 6 and 10 mm. The frame carrying the wire system (4×110 20 μm wires at a tension of 25 P) is attached with set (adjusting) pins to the foil frames, thereby guaranteeing the mechanical stability. Gas supply and electrical connections are similar to those of the prototypes. A photography of the whole detector unit is shown in fig. 10.

An extra chamber with an entrance window to enclose the detector has been constructed for use in a large scattering chamber. The mylar window is supported twice, – by a grid with a 2×2 division adjusted to the geometry of the detector, and a finer grid of 200 μm wires with a mesh-width of 15×15 mm^2. The window withstands a pressure difference up to 50 torr.

All electrical connections as well as those for gas supply and vacuum are fed through a flexible metal bellow connecting the detector chamber to the bottom platform of the large (3 m ∅) scattering chamber. Fig. 11 shows a photography of the whole set-up, the top part of the scattering chamber being removed. The counter can be rotated around the target and its distance changed by remote control. The supporting grids of the detector entrance window are easily recognized.

A total of 32 (16 anode- and 16 delay line-) signals are amplified in voltage sensitive preamplifiers, the 8 ΔE signals in charge sensitive preamplifiers, all situated close to the exit of the metal hose.

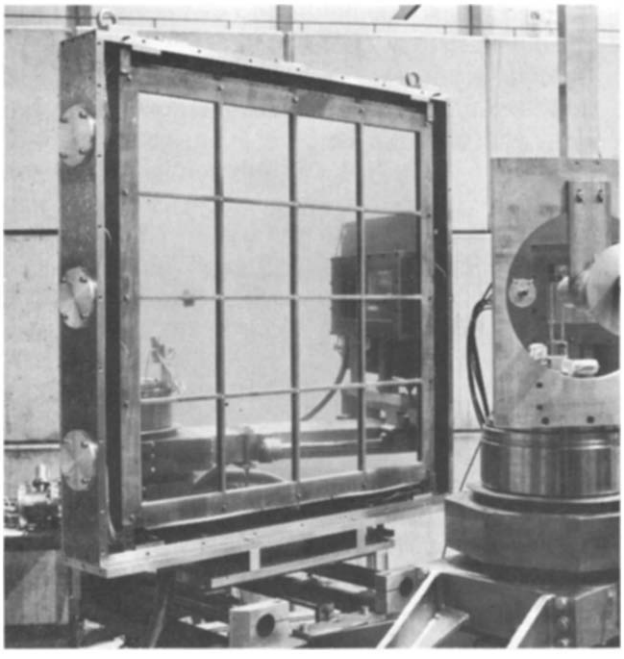

Fig. 10 Photograph of a square meter counter from the front side, the entrance window being removed The bellows on the bottom of the detector housing contain all connection cables, the gas-supply, and the by-pass to the vacuum system

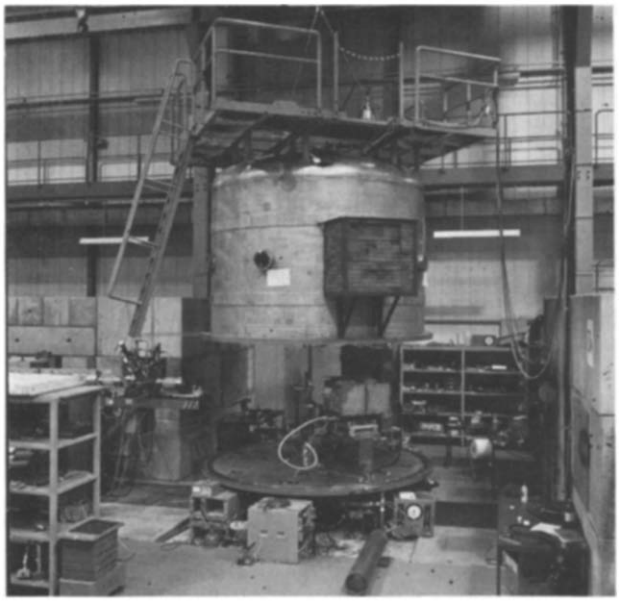

Fig. 11 Photography of the scattering chamber (3 m diameter) The top part is half-lifted The counters can be rotated and moved radially by remote control.

The rise time of the fast signals is found to be ~4.5 ns, slightly inferior to the prototypes as expected. By proper shaping, the base width of the anode signals can be reduced to 15 ns. The rise times of the delay line signals range from 5 to 18 ns.

The local time resolution as measured with elastically scattered heavy ions from Kr to U is about 240 ps, but degrades for the total area without geometrical correction to something like 700 ps. Spatial resolution is in any case estimated to be better than 1 mm, since the $d\bar{x}/dx$ modulations are clearly present.

5. Double event resolution and data processing

If only one particle at a time has to be analyzed in the whole detector, read-out and data processing are very simple. All logical time signals of one kind are fed via ORs into five TDC stop channels, started by the OR'ed anode signals from the first plane. All logical signals from the anodes are fed in parallel to a 16-bit pattern unit for reconstruction of the absolute coordinates.

The recognition and analysis of double or higher multiplicity events is much more elaborate. If one particle crosses the detector, two delay lines and two trigger planes are active. A second particle can be detected without any restrictions, if different trigger planes and delay lines are involved. For a random distribution of the second particle with respect to the first this applies to one half of the events, as can be visualized in fig. 12 (situation A). A more complicated case arises, however, if the two particles share one delay line but still have two different trigger signals (using both planes). At this

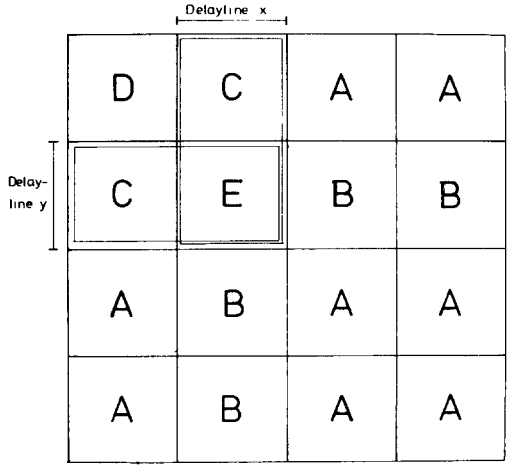

Fig 12 Double event distribution The first particle is assumed to be located in the section denoted by E There is no restriction for a second particle in sections marked with A For the sections marked with B and C one delay line is used in common with the first particle

point the double pulse resolution of the delay line has to be exploited. The situation is illustrated in fig. 13. The particles cross the detector at times t_1 and t_2 at coordinates x_1 and x_2, respectively. The two signals propagate to both ends of the delay line with the velocity $v(v = 1$ ns/mm), arriving with the time differences

$\Delta t_{\text{left}} = t_2 - t_1 + (x_2 - x_1)/v$

and

$t_{\text{right}} = t_2 - t_1 + (x_1 - x_2)/v$.

If one of these differences is larger than the typical double pulse resolution time of 30 ns, the second pulse can be analyzed. It is possible to reconstruct the event pairs t_1, x_1 and t_2, x_2, using two trigger signals and at least three delay line signals. This situation (B+C in fig. 12) applies to 37.5% of randomly distributed double events.

A special condition is met if two particles in the situation D of fig. 12 cross the detector at exactly the same time. In this case, no decision can be made on whether the coordinates combine in the form x_1, y_2 and x_2, y_1, or x_1, y_1 and x_2, y_2. Because of the 6% probability and the equal trigger times this only rarely occurs.

The most complicated case is met in situation E of fig. 12 where the same trigger planes and delay lines are involved. The two events can then only be resolved, if either their time difference is larger than the double pulse resolution of the anode signals (about 18 ns), or of their spatial separation in both coordinates is larger than 5 cm, resulting in 2

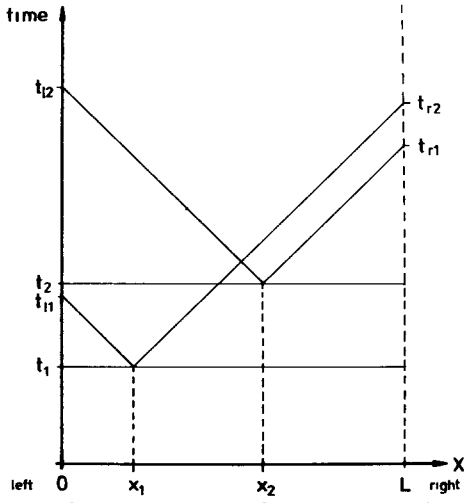

Fig 13 Reconstruction of double events from one delay line Starting from two events $(x_1 t_1)$, $(x_2 t_2)$, four signals propagate to the delay line ends. Time differences with the trigger signals t_1, t_2 are measured. A computer program checks for the proper signal pairs (right–left). The sum of two adjacent time differences must correspond to the total delay.

trigger signals and 8 different position signals to be usable for complete reconstruction.

Double pulse resolution does not only depend on the rise time and base width of the signals, but also on the dead time of the CFT, set in our case to 12 ns for the anode signals and 24 ns for the delay line signals. It is, in any case, necessary to split up the two consecutive logical signals and feed them into two different time analyzing channels. This is achieved by a fast selfswitching multiplexer which delivers the first pulse on channel 1 and the second and all following pulses on channel 2, conserving the time information.

In principle, a complete data processing system for double events can be built by using two time to digital channels for each anode and delay line signal resulting in a total of 64 TDC channels. However, a double event is completely defined by only 12 signals and all information can already be obtained using only 12 TDC channels. In this case extensive gating or demultiplexing becomes necessary.

We have developed a demultiplex unit reducing the number of TDC channels to 16, i.e. two 8-fold TDCs and two 16-bit pattern units are used for complete determination of double events. The unit accepts the logical signals from the anodes and the delay lines of one plane. It delivers triples (anode, delay line 1, delay line 2) of fast signals and 8-bit pattern bytes for three different priorities. The earliest particle is gated to the priority I outputs, etc. If two signals arrive within a time interval smaller than some limit, the higher priority is given to the lower pattern bit.

The fast signals are splitted, one is then used to perform logical operations, i.e. setting of gates according to priority, the other is cable delayed and gated to a few outputs retaining its timing information.

The two TDC-modules are used as follows

1st Plane		2nd Plane
Anode Prio I	Start	Anode Prio I
Anode Prio I-double	Stop 1	Anode Prio I-double
Anode Prio II	Stop 2	Anode Prio II
Right Prio I	Stop 3	Up Prio I
Right Prio I-double	Stop 4	Up Prio I-double
Right Prio II	Stop 5	Up Prio II
Left Prio I	Stop 6	Low Prio I
Left Prio I-double	Stop 7	Low Prio I-double
Left Prio II	Stop 8	Low Prio II

The gating unit has two cycles. During the opening cycle the unit accepts fast input signals. It is defined by the first fast signal and a monoflop. The

length always has to be adjusted to the specific experimental conditions. If the event has been accepted by the experiment logic the unit holds information until the computer reset has occured. If not a fast reset is transmitted to the priority unit which is then ready to accept a new signal. The maximum count rate depends on the time needed by the experiment logic for the decision, whether the presented signal is acceptable or not. If this time is 300 ns, an instantaneous rate 3×10^5 is possible.

6. First experiments and calibration

The square meter detector has been used in several experiments for the detection of sequential fission fragments emerging from reactions like 7.5 MeV/amu U, Pb → Ni, Zr, Pb, U. In these measurements the target-like reaction product is detected in a position sensitive ionisation chamber[1]). The large area detector is positioned to detect a coincident projectile-like reaction product in about its center. A photograph of the whole set-up is shown in fig. 14. If binary fission of the projectile-like nucleus occurs sequentially as a second reaction step the possible lab directions of the two fragments are compressed within a cone centered around the original direction. The opening angle of this cone depends on the magnitude of the relative velocity of the fission fragments compared to the velocity of the fissioning system. By adjusting the distance of the detector, the whole projection of the cone can be covered simultaneously within the active counter area. The two fragments then appear in a correlated way which usually corresponds to situation A (no restriction) in fig. 12. There is, however, a considerable probability for situation B (same delay line) due to a finite spreading of recoil directions. Fig. 15 shows a distribution of fission (two fragment) events in coincidence with a Zr-like nucleus from the reaction Pb → Zr at 7.5 MeV/amu. Results of these measurements will be published elsewhere[18,19]).

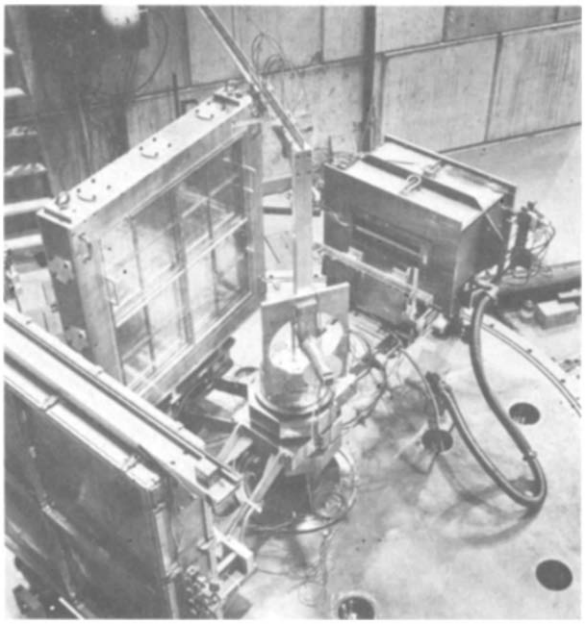

Fig 14 Experimental set-up for the measurement of sequential fission induced by U and Pb on lighter targets like Ni, Zr The target-like recoil particle is analyzed in the ionization chamber on the right, the two fission fragments are measured simultaneously in the large area detector on the left The movable Faraday cup (trifilar mount) can be seen in the center of the picture

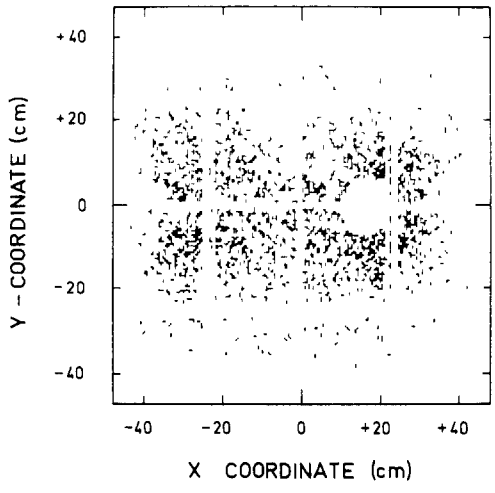

Fig 15 Spatial distribution of two fission fragments in coincidence with a recoil particle measured in the ionization chamber The shadow of the support grid and of the Faraday cup can readily be recognized The concentration of events in the equator zone is due to the high angular momentum transfer of the reactions

For successful data reduction proper calibration procedures have to be applied both for the spatial coordinates and for time of flight. Since all relevant quantities appear as time differences, only time offsets have to be determined. For the calibration of the spatial coordinates a plate with a regular hole pattern (∅ 3 mm) is placed in front of the detector. This pattern then has to be reconstructed on the computer screen. For the determination of time offsets one makes use of the pulsed beam of the UNILAC ($\Delta t \lesssim 200$ ps) together with the well defined behaviour of elastic scattering is utilized. The detector center is positioned at or near 0° (only

events more forward than the grazing angle are useful), with a movable faraday cup in front. By changing the distance of the cup relative to the target, the intense central zone of the Rutherford scattering distribution is shadowed most of the time in order to obtain a more even distribution of the local dose. Time offsets are then determined by a computer program which adjusts them locally to reproduce the elastic scattering velocities: A map of time offsets is then obtained as a function of coordinates. Unexpectedly, time offsets within one trigger module ($22 \times 44\ \mathrm{cm}^2$) do not follow a simple geometrical spatial dependence: A minimum time delay is found for events in the center, rising monotonously towards all edges, even in the direction of a contact. Maximum differences within one module are of the order 1.5 ns. Although this behaviour is not understood in detail, a qualitative interpretation can be given. Consider a parallel strip counter of length L with one end matched to a cable and the other end left open. If a particle crosses at position x, a direct signal will reach the cable at the time $t_1 = x/v_s$, v_s being the propagation velocity. A second signal propagates in the opposite direction, is then reflected at the open end at time $t_2 = (L-x)/v_s$, and reaches the cable at time $t_2' = (2L-x)/v_s$. If filtering and trigger mode correspond to mean timing, the time delay is independent of x.

Such considerations, taking also account of the second dimension, together with damping and improper matching, may explain the observed effect.

7. Conclusions

We have demonstrated the possibility to build, operate and ultimately extract data from a square meter time-, position- and ΔE-sensitive heavy ion detector. The outstanding properties of a parallel plate counter have been expanded by position sensitivity without affecting time resolution. The collective read-out with direct coupled delay lines of $\tau = 1$ ns/mm has the virtues of

1) inherent interpolation and excellent integral linearity,
2) double pulse resolution of 25–30 ns (25–30 mm),
3) redundancy and simple pile-up rejection,
4) simple calibration and data extraction.

The use of two independent, but identical detector planes for x and y determination has the following advantages:

1) rejection of noise, electron- or γ-pulses,
2) determination of time resolution independent from the pulsed beam,
3) resolution of pulse number ambiguities in pulsed beam experiments,
4) improved multiparticle event resolution,
5) simple and cheap possibility of adding ΔE sensitively with one additional grid.

A number of variations of the principle are possible for special applications. A reduction of the gap width will increase the time resolution to about 150 ps. A reduction of the ratio wire distance to gap width may dramatically improve the differential linearity (fig. 5). Thin foils ($< 100\ \mu\mathrm{g/cm}^2$) may extend the dynamical range to very low ion energies and reduce straggling. Such a detector can then be used as a transmission counter in front of an ionization chamber. For high count rate applications pile-up probabilities can be reduced by lowering the maximum delay for the position signals. This can be achieved either by reducing the delay time per mm, or reducing the number of wires being collectively read-out with one delay line.

We gratefully acknowledge valuable contributions of P. Glässel, R. Männer, and W. Schneider during the actual experiments and the data reduction. We are also indebted to H. Gemmeke and W. Farr for their help in the development of the electronics.

References

1) H Sann, H Damjantschitsch, D Hebbard, J Junge, D Pelte, B Povh, D Schwalm and D B Tran, Nucl Instr and Meth. **124** (1975) 509
2) R Albrecht et al , GSI-Bericht P-2-74 (Sept 1974)
3) B Martin et al , to be published
4) P Armbruster, J de Phys **37** (1976) C5-161
5) R. Albrecht et al Jahresbericht MPI Heidelberg (1975) p 21, S Bohrmann, Diplomarbeit (Universitat Heidelberg, 1976)
6) D v Harrach, Jahresbericht MPI Heidelberg (1976) p 24, J Lauer, Diplomarbeit (Universitat Heidelberg, 1976)
7) Y Eyal and H Stelzer, Nucl Instr and Meth **155** (1978) 157
8) J Christiansen, Z angew Phys **4** (1952) 326
9) A Krusche, D Bloess and F Munnich, Nucl Instr and Meth **51** (1964) 197.
10) J E Draper, Nucl Instr and Meth **30** (1964) 148
11) H J Specht, Berichte der Kernforschungsanlage Julich-Jul-Conf-4 (1970) pp 71-120
12) H Stelzer, Nucl Instr and Meth **133** (1976) 409
13) G. Gaukler, H Schmidt-Bocking, R Schuch, R Schulé, H J Spect and I Tserruya, Nucl Instr and Meth **141** (1977) 115
14) H Brosicke, Diplomarbeit (Universitat Heidelberg, 1976)

15) M Just, D. Habs, V Metag and H J Specht, Nucl Instr and Meth. **148** (1978) 283.
16) J Schukraft, D Habs, D v. Harrach, J Lauer, V. Metag and H J Specht, Jahresbericht MPI Heidelberg (1977) p. 52
17) D v Harrach, R. Männer, W. Schneider and H. J Specht, Jahresbericht MPI Heidelberg (1976).
18) H J. Specht, Proc. Int. Conf. on *Nuclear interactions*, Canberra (1978); Bericht MPI Heidelberg V26 (1978).
19) D. v Harrach, P Glassel, Y. Civelekoglu, R Männer and H. J Specht, Phys. Rev. Lett **42** (1979) 1728